Origin of the low-energy gamma ray flux of the long-lasting thunderstorm ground enhancements

A. Chilingarian,[1,2,3] A. Avetisyan,[1] G. Hovsepyan,[1] T. Karapetyan,[1] L. Kozliner,[1] B. Sargsyan,[1] and M. Zazyan[1]

[1]*A. Alikhanyan National Lab (Yerevan Physics Institute), Yerevan 0036, Armenia*
[2]*National Research Nuclear University MEPhI, Moscow 115409, Russia*
[3]*Space Research Institute of RAS, Moscow 117997, Russia*

(Received 4 February 2019; published 14 May 2019)

To identify the role of the gamma radiation from radon progenies in long-lasting thunderstorm ground enhancement (TGE) flux, the differential energy spectrum is measured with various spectrometers, including precise spectrometer of ORTEC firm built with 3"×3" inches sodium iodide NaI(Tl) crystal; full width at half maximum (FWHM) ∼7.7% at 0.6 MeV. The measurements demonstrate that radon progeny radiation significantly contributes to the count rate enhancements measured in the winter of 2018–2019 in the energy range below 3 MeV. However, performed Monte Carlo simulations and observation of long-lasting TGEs with plastic scintillators of various thicknesses and energy thresholds show that TGEs originate in the intracloud electric fields. Radon progenies (mostly ^{214}Bi spectral lines) contribute to count rate in the low-energy domain.

DOI: 10.1103/PhysRevD.99.102002

I. INTRODUCTION

The emerging field of high-energy atmospheric physics (HEAP) [1] studies processes producing high-energy particles in the terrestrial atmosphere, such as thunderstorm ground enhancements (TGEs) [2,3], terrestrial gamma ray flashes [4], and gamma ray glows [5,6]. Understanding these phenomena requires developing appropriate models of the interaction of electrons, positrons, and photons with air and electric fields [7–9]. It is widely accepted that all three processes are mainly driven by electric fields, ionization, scattering, and bremsstrahlung. One of underlying processes, namely, runaway breakdown (RB) [10], now mostly referred to as relativistic runaway electron avalanche (RREA) [11,12] is a "threshold" process controlled by the strength of the electric field. RB/RREA is responsible for the development of electron–gamma ray avalanches in the atmosphere and, consequently, for the large-scale multiplication of the particles detected on Earth's surface or observed in the atmosphere by spectrometers located on balloons and aircraft. The second process, modification of the electron energy spectra (MOS) [13,8], operates on much lower scales; however, it is effective for almost all strengths of atmospheric electric fields.

Although many TGEs have been observed in mountaintop and sea-level experiments (see references in [14]), the spatial structure of electric fields and the time evolution of electron acceleration in the atmosphere are poorly understood. The "electric" origin of the ionization radiation from clouds itself is sometimes put under question. Bogomolov *et al.* [15] argue that the significant contribution to the low-energy part of the TGE spectrum is originated by the Rn-222 decay chain, including daughter isotopes ^{214}Bi and ^{214}Pb that are clearly identified in the spectrum of the background radiation. Although we demonstrate that the hypothesis of the precipitation as a source of gamma ray radiation is not valid [16], it was proposed that Rn-222 can be concentrated in the clouds above Aragats research station and radiation of Rn-222 daughter isotopes can comprise the low-energy part of TGE [15].

However, recent measurements by Armenian and Japanese researchers [17,18] have revealed many more details about the relations of TGEs and electric fields inside the cloud. Numerous TGEs observed on Aragats are an ideal target to investigate the source of the ionization radiation from the clouds because the low altitude of thunderclouds enables us to detect electrons, gamma rays, and neutrons simultaneously [2,3] and to observe each individual avalanche originated by a cosmic ray (CR) electron (seed particle) entering a high-electric-field region [19]. The interplay of TGEs and lightning flashes (see [20], Figs. 6 and 7) also shows the ultimate causal relation and dependence of TGEs on atmospheric electric fields.

Unstable nuclides comprise a significant portion of the low-energy gamma ray flux measured by particle detectors and spectrometers at Aragats station. Fair weather (background) gamma ray energy spectra measured on Aragats Mountain are a mixture of the continuous spectrum produced by Galactic (and, sometimes, also solar) cosmic rays in interactions with the atmosphere and emission lines of several isotopes (lines are turned to distributions with finite width dependent on the spectrometer resolution). It is very difficult to see any "isotope-produced" structures in

the resulting spectra of TGE with low-resolution large-size spectrometers used for the 24-7 monitoring of gamma radiation at Aragats (see details of the NaI spectrometer network at Aragats in [20,21]). To measure the contribution of the gamma radiation from radioactive isotopes, we perform the following program of measurements with a high-resolution spectrometer that began operation at Aragats in December 2018:

(i) Analyze the background radiation spectrum measured at Aragats and in Yerevan by precise ORTEC spectrometers;
(ii) Investigate the fluctuations of the measurements of spectral lines ^{214}Bi (0.609 MeV) and ^{40}K (1.46 MeV) with the precise spectrometer located indoors and in the open air;
(iii) Present results of Monte Carlo modeling of the MOS process, as an origin of the long-lasting TGE.
(iv) Critically examine the methodology of the recovering of energy spectra and evaluate emerging methodical errors.
(v) Perform analysis of the gamma ray flux enhancements observed in the winter of 2018–2019 with an emphasis on the most pronounced spectral lines, namely, ^{214}Bi (0.609, 1.12, and 1.76 MeV).

II. POSSIBLE SOURCES OF LOW-ENERGY (BELOW 3 MEV) GAMMA RAYS REGISTERED ON EARTH'S SURFACE

Natural radioactivity measured on Earth's surface can be explained by the following main sources:

(1) Rather stable primary particle flux coming mostly from supernova explosions in our Galaxy and from numerous extra-Galactic sources. Neutrinos, gamma rays, and ultrahigh-energy nucleons can come from very distant violent explosions in the Universe (like neutron star mergers or black hole jets). CR particles incident on Earth's atmosphere originate in the atmosphere's extensive air showers (EASs) containing billions of electrons, muons, and gamma rays. Thus, EASs sustain rather stable energy spectra of these and other species of CR specific for each geographic coordinate (yes, meteorological effects can modify the spectra in the low-energy domain).
(2) Transient radiation from periodically activated solar accelerators.
(3) Cosmogenic nuclides that are generated by the nuclear reactions during the interaction between cosmic radiation and stable isotopes in the atmosphere (for example, ^{14}C and ^{3}H).
(4) Long-lived unstable nuclides (^{238}U, ^{235}U, ^{232}Th, ^{40}K, etc.) that originated in neutron star (or neutron star and black hole) mergers. The original radionuclides disintegrate to the secondary radionuclides and form the decay chains, i.e., the uranium-radium decay chain (starting from ^{238}U to ^{226}Ra, ^{222}Rn, ^{218}Po, ^{214}Bi…); thorium decay chain (starting from ^{232}Th to ^{224}Ra, ^{222}Rn, ^{212}Pb, ^{212}Bi…); and actinium decay chain (starting from ^{235}U to ^{223}Ra, ^{219}Rn, ^{211}Bi…), that are present in the open air. Several isotopes emit radiation in form of gamma rays (spectral lines). However, depending on the limited resolution and sizes of the spectrometers, these lines broadened and are seen as more or less pronounced peaks with finite width. For the measurements with large crystals, spectral lines are smoothed and the contribution from isotope decay we can notice only as a broad bump at low energies.
(5) Additional radiation from the CR electrons accelerated in the emerging in atmospheric electric fields. Gamma ray emission is governed by RB/RREA and MOS processes. Both processes originate continuous spectra of gamma rays in the energy range 0.3–100 MeV.
(6) Additional radiation in the 0.3–3 MeV range from unstable nuclides occurring during TGEs. From this process, we can expect the enhanced intensity of spectral lines.

The first manifestation of TGE is a large narrow (for the detectors with a high energy threshold) or broad (for the detectors with a low energy threshold) peak in the time series of count rates (see Figs. 4 and 9 of [16]). As a rule, in the same time we observe a huge storm with many lightning flashes and disturbances of the near surface electric field (see Figs 1 and 3 of [16]). In the TGE analysis procedures, we select the minutes to recover energy spectra (usually at and around the location of the largest peak; see, for instance, Fig. 5 in [20]). The techniques of differential energy spectra recovery is described in the Instrumentation section of [20]. The most important issue in recovering TGE energy spectra is to obtain as much "pure" signal as possible without background contamination to avoid "fake" peaks. We have to use measurements of the "stable background" just before TGE and subtract it from the minutes when the peak is detected. Then, we look for the significant enhancements in the intensity of spectral lines in the histogram obtained after subtraction, calibrate, enumerate the peaks' position and intensity, etc. These techniques should work perfectly if the background (points 1–4) is stable. Unfortunately, CR radiation (point 1) cannot be accepted as stable in the low-energy range (below 3 MeV). The meteorological effects (atmospheric pressure and temperature gradient in the atmosphere; see [13]) can highly change the low-energy particle flux. The radiation from unstable isotopes on Earth's surface (point 4) is also very variable, changing significantly on the hour-to-hour scale due to the same meteorological effects when the spectrometer is located outside (the case for the spectrometer used in [15]).

Thus, proving the origin of flux enhancement in the low-energy range is a very difficult task. Usually, we would make a trade-off between statistical significance and

possible biases of background spectra estimates. Due to the small size of the NaI crystal ($5 \times 5 \times 5$ cm) of the spectrometer, 50 minutes' data collection time was required to get appropriate statistical significance [15]. The sample of the pure background was accumulated during 50 minutes before start of the particle flux enhancement. However, as mentioned above, due to the high variability of isotope concertation in the air, in these two samples the mean intensity of the background can be different, leading to fake peaks.

Radon (^{222}Rn) is the immediate daughter of ^{226}Ra and is continuously produced wherever ^{226}Ra exists. ^{226}Radium is itself abundant in rocks and soils and in the materials derived from them. Because it is a noble gas, radon is relatively much more free to migrate than either its parents or daughters, all of which are metals.

The half-life of the radon isotope ^{222}Rn is 3.82 days; thus, it can be transported to the atmosphere due to the diffusion mechanism. Mean concentrations of radium can be assumed to be constant on Aragats, a research station surrounded by rocks; however, the concentration of daughter nuclides in ambient air should follow strong variations due to fast-changing meteorological conditions. The ratio of maximum to minimum diurnal variations of the atmospheric radon measured in four countries is approximately in the range of 2–5 [22]. The concentration of ^{222}Rn in surface air was measured in 1989 at Sacavem-Lisbon, Portugal. At the sampling station, located at 38° 47'N 09° 06'W, concentrations of radon strongly fluctuated between 1 and 40 Bqm^{-3} [23]. The average daily course of ^{222}Rn concentration measured during the years 1991–1994 in Bratislava, Slovakia, has a waveform with a maximum between 4 and 6 a.m. and with a minimum between 2 and 4 p.m. [24]. The ratio of the maximum to minimum radon equals 1.7. The variation of the indoor radon concentration is much smaller, being maximal in the basement and decreasing at higher floors of the building. Atmospheric radon exhibits a vertical concentration profile which normally ranges from a maximum at the air-soil interface to an immeasurably low value in the stratosphere [22]. The vertical profiles of ^{222}Rn concentration measured by aircraft flying above the west-central portion of the continental United States demonstrate a rapid decrease of concentration with altitude (see Fig. 3 in [25]).

Thus, world data on radon concentration in the atmosphere demonstrate large variability during the day, fast decline with altitude above Earth's surface, and a decrease with the outside temperature.

III. NATURAL GAMMA RADIATION MEASUREMENTS ON ARAGATS AND IN YEREVAN WITH HIGH-RESOLUTION SPECTROMETERS

To investigate the hour-to-hour variations of radon progenies and enumerate the spectral lines, we perform monitoring of the natural gamma radiation (NGR) of a Rn-222 daughter chain on Aragats and in Yerevan with ORTEC firm spectrometers [26]:

(i) NaI(Tl), type 905-4 (ORTEC), 3"×3" diameter and length), 1024 channels, very high stability, maestro software for spectral lines identification, with relative energy resolution (FWHM ∼7%)

(ii) High-purity germanium (HPGe) coaxial detector system, Model GEM15P4-70 (ORTEC), with relative energy resolution (full width at half maximum (FWHH) ∼1%)

The goal of measurement was to measure the diurnal variations of the background on Aragats in the building where the NaI network is located and outdoors near the spectrometer used to obtain the data plotted in Fig. 2 of [15]. In Fig. 1(a) we show the background spectrum measured at Aragats beneath the roof of the SKL experimental hall. In Fig. 1(b) we show the background spectrum measured in

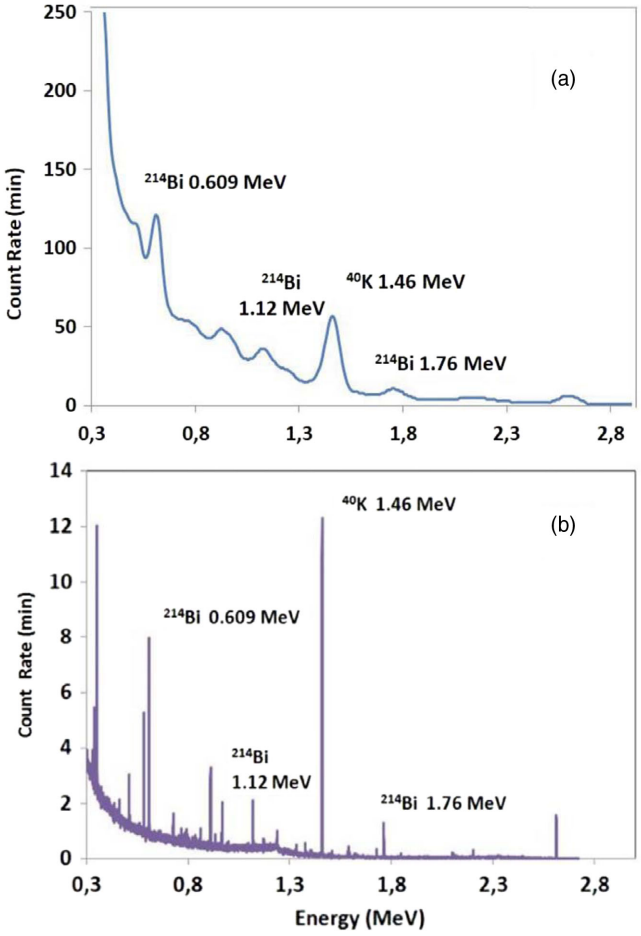

FIG. 1. Indoor background gamma ray energy spectrum measured at Aragats and in Yerevan with various spectrometers: (a) NaI (Tl) and (b) HPGe. The ^{214}Bi spectral line (peak) will be used for the investigation of diurnal variability of radon concentration at Aragats. We also consider the potassium ^{40}K isotope as a stable spectral line used for the calibration of fast varying ^{214}Bi spectral lines.

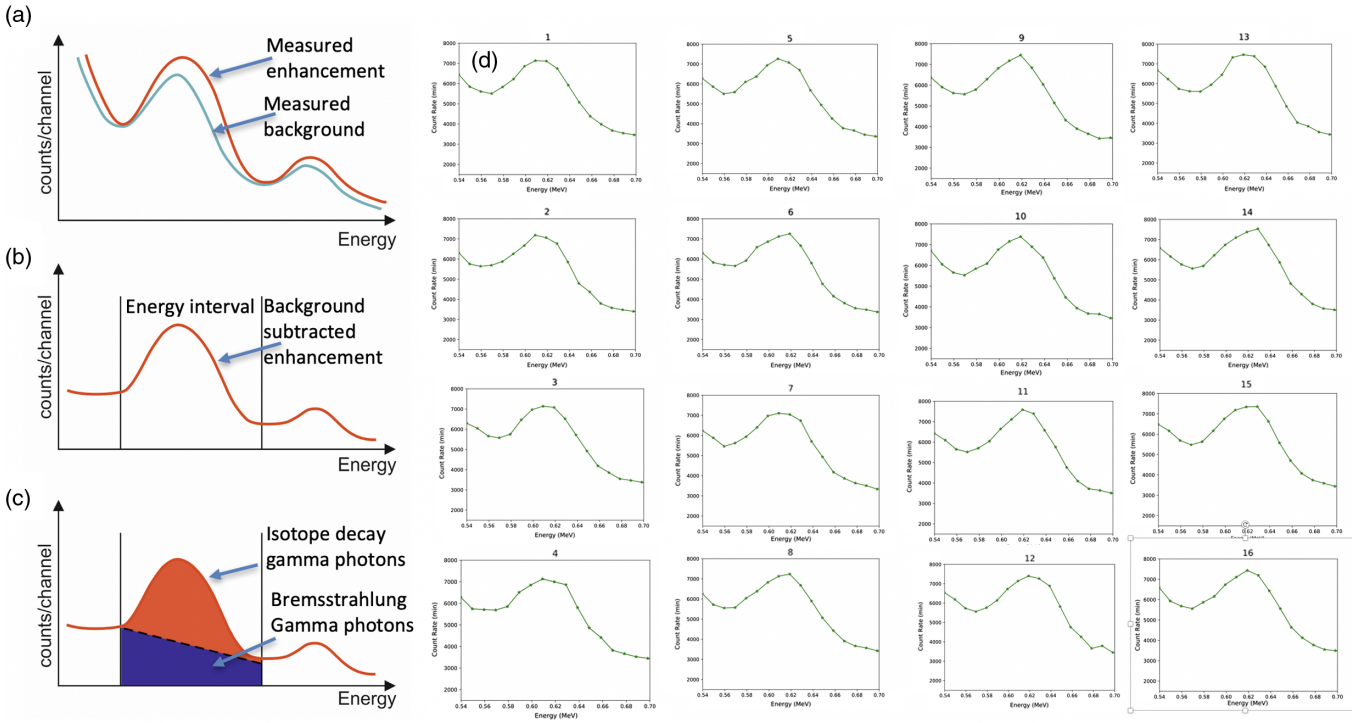

FIG. 2. Illustration of the standard procedure of the background extraction and spectral peaks area calculation [(a), (b), and (c) are modified from [27]] and routinely measured 1-hour histograms of the spectral line 0.609 MeV from ^{214}Bi decay enumerated by the NaI (Tl) ORTEC spectrometer (d).

Yerevan indoors by a high-resolution HPGe spectrometer (to be transported to Aragats in the spring of 2019). The overall picture of the ^{238}U chain isotope gamma radiation is very well expressed by the measurements made by the HPGe spectrometer. HP Ge spectrometer resolved very close ^{214}Bi and ^{214}Pb decay spectral lines; these two NaI(Tl) spectrometer measured as one broad peak at 0.609 MeV (the same peak as in Fig. 2 in [15]). We will use this peak, which was claimed to have maximal significance in [15] for measurements of the diurnal variations.

The recovery of spectral lines was performed according to the standard procedure used in isotope spectroscopy [27].

After measurement of the energy spectra, we choose the spectral line and outline the energy window around the peak. Then, we subtract the background measurement taken just before TGE and from the histogram corrected in this way we calculate the peak area as demonstrated in Fig. 2(c). For investigation of the diurnal and daily variations of the 0.609 MeV spectral line, we omit the procedures shown in Figs. 2(a) and 2(b).

In Fig. 3 we demonstrate diurnal variations of the count rates of joint ^{214}Bi and ^{214}Pb decay gamma rays measured by NaI(Tl) spectrometer (in the energy range 0.56–0.66 KeV). By diamonds, we show the diurnal variation of the NaI (Tl) spectrometer positioned under the roof of the SKL experimental hall where the Aragats NaI network is located. As demonstrated in [22], the indoor radon concentration fluctuations have a vertical negative gradient. The fluctuations of ^{214}Bi are much larger for the outdoor location of the spectrometer (the relative range is ∼47%); for the indoor location, in the highest position in the building, while the concentration is much higher but also much more stable (the relative range is ∼12%). Thus, the location of the NaI network at the maximal height in the building provides minimal diurnal variations. The open-air location of the same spectrometer near the spectrometer used in [15] leads to

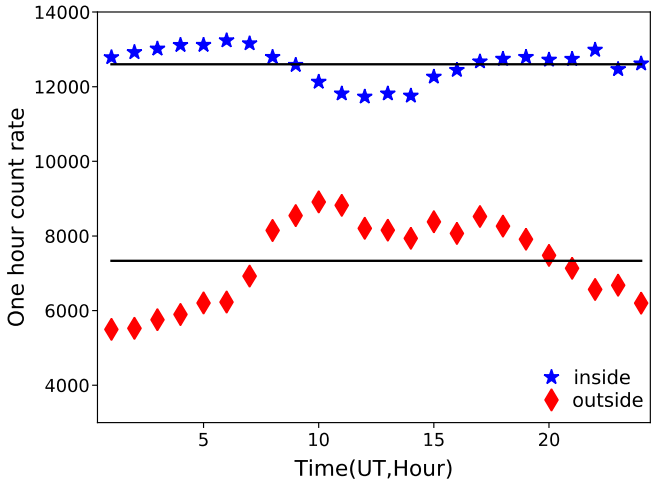

FIG. 3. Diurnal variations of the intensity of the 0.609 MeV (^{214}Bi) spectral line measured indoors and in the open air, from measurements performed in December 2018.

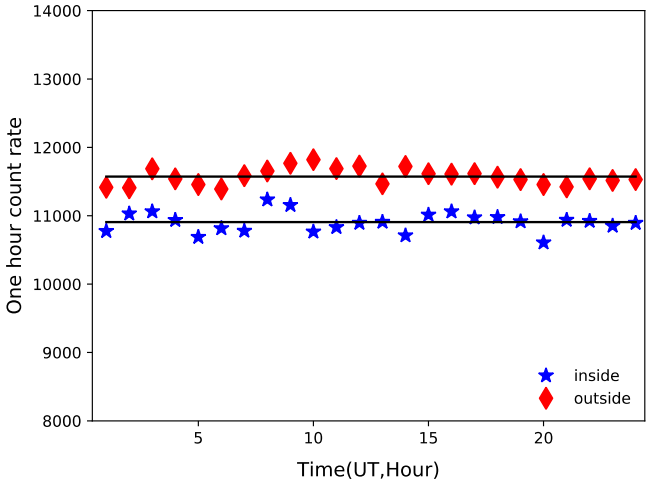

FIG. 4. Diurnal variations of the intensity of the 1.46 MeV (potassium-40) spectral line measured indoors and in the open air.

much larger diurnal variations (diamonds in Fig. 3) as is expected from world data on radon concentration (see references in the previous section).

Potassium-40 (^{40}K) is a radioactive isotope of potassium which has a very long half-life of 1.25×10^9 years. It makes up 0.012% of the total amount of potassium found in nature. It decays to the gas argon-40 by electron capture with the emission of an energetic gamma ray of 1.46 MeV energy. Potassium-40 assimilates into the materials derived from rock and soil.

As we can see in Fig. 4, potassium-40 concentration does not vary with daytime and does not depend strongly on atmospheric conditions. The fluctuations of potassium-40 indoors and outdoors are approximately the same; the relative range is 5.8% and 3.7% correspondingly. As the 1.46 peak is always present in the natural gamma ray energy spectrum, it can be used for the calibration purposes.

Large fluctuations of the ^{214}Bi spectral line (Fig. 3) pose limitations on the possibility of physical inference on the radon origin of TGE based on the observed peak in [15]. The enhancement of the gamma ray flux registered by spectrometers (signal) started at t1 can be attributed to several physical processes, foremost of which are summarized in Eq. (1):

$$S_{t1} = S_{AV} + S_{MOS} + S_{Rn} \pm S_M, \tag{1}$$

where S_{AV} is an intense gamma ray flux due to the electron-photon avalanche process started in the strong atmospheric electric fields; S_{MOS} is bremsstrahlung gamma ray flux also released in the atmospheric electric fields of much lesser strengths; S_{RN} is due to radon daughter isotope radiation from the clouds above the detector site, or from another yet unspecified source; and S_M is the influence of different meteorological effects (atmospheric pressure, gradient of temperature, etc.). For identification of the possible signal from radon progenies, the statistical fluctuations can be substantial. As we demonstrate in Fig. 2, the standard technique of the spectral analysis is subtraction of the background measured separately before TGE. See Eq. (2), where we denote by ON the sample containing background with possible signal and by OFF the pure background:

$$ON = S_{T1} + B_{T1}; \qquad OFF = B_{T2}. \tag{2}$$

However, by subtracting *OFF* sample from *ON* sample, we do not obtain "pure" signal. To collect enough events, the time span Δ_T started at T_1 and T_2 is rather large (50 minutes to obtain Fig. 2 in [15]), and due to large fluctuations of the count rate measured by the gamma spectrometer located on open air (see Fig. 3(b)) $B_{T1} \neq B_{T2}$; see Eq. (3):

$$ON - OFF = S_{T1} + B_{T1} - B_{T2} \neq S_{T1}. \tag{3}$$

Due to hourly fluctuations of the radon concentration in the atmosphere, we can obtain a "fake" signal of ~5–10% only because of the difference in background samples measured starting at T1 and T2 times. The fluctuations of the count rate measured by the spectrometer used in [15] are large and ^{214}Bi peaks are not well pronounced because of the small size of the NaI(Tl) crystal used in their spectrometer. The NaI crystal is very sensitive to the temperature and responds nonlinearly on solar heating. Therefore, the energy spectra of gamma rays should be measured indoors on the highest floor of the building where radon concentration is minimal. The NaI network used for recovering the energy spectrum is located indoors where fluctuations of background are minimal (see Fig. 3). Due to the large size of the NaI crystal, the background sample is collected during just a few minutes before the event and large fluctuations are not probable. Usually during TGE we register large energies of gamma rays far beyond the ones possible from any radioactive decay. Additionally, to prove the "electric" origin of TGE we perform a cycle of simulation experiments, described in the next section.

IV. MODELING OF THE RB/RREA AND MOS PROCESSES IN THE ATMOSPHERE TO REVEAL FEATURES OF THE GAMMA PHOTON SPECTRUM MEASURED ON EARTH'S SURFACE

The atmospheric gamma ray energy spectrum initiated by extensive air showers is usually presented within a model based on a power-law continuum (index of −1.16 in the few MeV energy range [28]). Gamma ray flux measurements clearly reveal the 511 KeV line due to the annihilation of positrons produced in EASs. After our observation of long-lasting TGEs [17], extending the flux

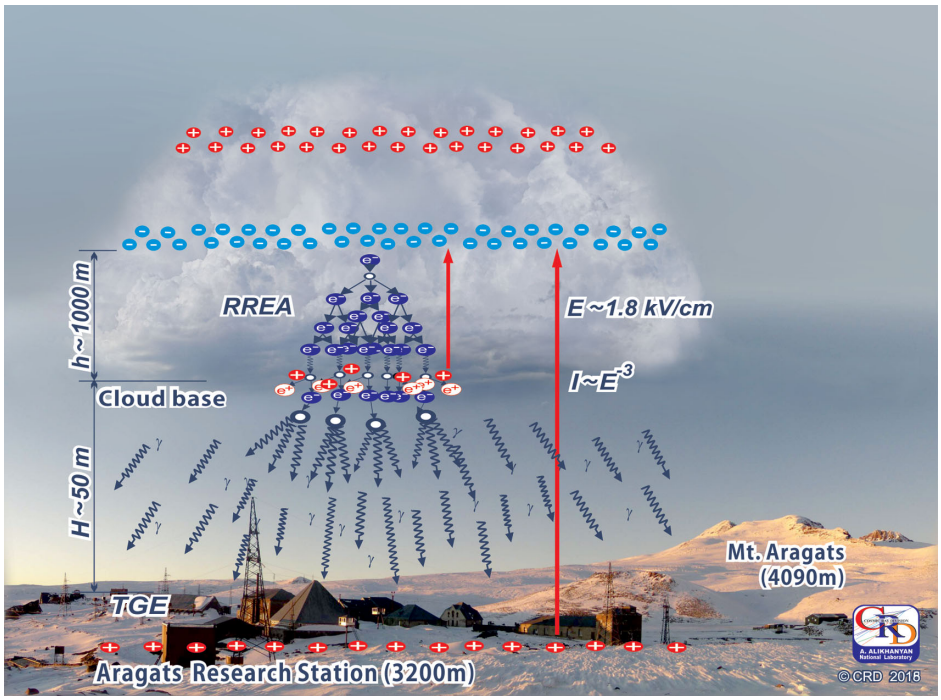

FIG. 5. The scheme of electron acceleration modeling in the atmosphere.

of gamma rays observed at Aragats up to several hours, we started a cycle of simulations to find out how electric fields of different strengths and elongations can modify the gamma ray spectrum in the atmosphere. The main goal of Monte Carlo simulations was to determine if the MOS process [14] can provide such a long-duration gamma ray flux; if remote extensive cloud showers (ECSs) can contribute to this flux; or if we should consider another origin of gamma rays, say, radon progeny gamma radiation (or if all processes have a part in the additional particle flux). Thus, our simulations are always pairing with observations and with hypothesis testing.

For a new series of simulations, we use the CORSIKA package; see details of the options of CORSIKA code in [29]. From the consideration of the ~500 TGE events in the last decade, we conclude that not all TGEs are due to the intense RB/RREA process; for instance, winter TGEs were not accompanied by thunderstorms and large disturbances of the near-surface electric field. To investigate the "small fields" effect that is typical for winter TGEs, we use in simulations rather low values of the atmospheric electric field strengths starting from 0.1 MeV/cm. The overall scheme of the simulations is presented in Fig. 5.

Each simulation set consists of 10^8 showers originated from vertically traversing CR electrons with energies in the interval $1 - 300$ MeV. The differential energy spectrum of electrons follows the power law with spectral index $\gamma = -1.21$. Avalanche particles were followed to Earth's surface ($H_{obs} = 3200$ m a.s.l.) or until their energy became less than $E_{cut} = 0.05$ MeV. Electric field $Ez > 0$ was introduced a kilometer above the "cloud base" H that was changed from 50 to 1000 m.

As we can see in Fig. 5, two fields are supporting electron acceleration downwards: the field between the main negative layer and its mirror on Earth and the field between the same negative layer and small positively charged layer in the bottom of the cloud. It is a highly simplified structure; however, the most intense TGEs happened when both fields were in play and their superposition exceeded the avalanche initiating threshold. In the simulation, we assume no difference between these fields and the existence of a constant field with the length of 1 km and a fixed prechosen strength. Such a field elongation and strength were both routinely measured in balloon flights [30,31].

In Table I we enumerate the gamma ray flux enhancement in the electric fields of different strengths. After reaching the RB/RREA threshold, the number of particles exponentially rose in the electron–gamma ray avalanches. However, even for the small electric field we have a significant enhancement that can be reliably registered by the spectrometers and counters located on Aragats.

In Table II we post the particle flux enhancement (comparing with fair weather values) in different energy intervals. We see that most of the enhancement occurred at low energies (0.3–2 MeV).

In Table III and Fig. 6 we demonstrate the influence of electric field height on the number of additional gamma rays reaching Earth's surface decreases twofold, and for 1000 m this number is three times less. We can see that when the distance of the electric field from particle

TABLE I. The number and relative enhancement of secondary photons reaching Earth's surface after traversing the electric field of 1 km located 50 m above Aragats research station (3200 m a.s.l.).

Ez (kV/cm)	N(Ez)	(N(Ez)-N(0))/N(0) (%)
0	370647	0
0.1	387271	4.5
0.2	405065	9.3
0.3	425962	14.9
0.9	626225	69.0
1.7	1879136	407.0
2.0	9052389	2342.3

TABLE II. Enhancement [N(Ez)-N(0))/N(0) (%)] of secondary photons in different energy intervals.

Ez (kV/cm)	0.3–2 MeV (%)	50–60 MeV (%)	70–80 MeV (%)
0.1	5.6	5.7	3.7
0.2	11.3	7.4	3.7
0.3	17.7	11.8	4.7
0.9	82.9	37.1	32.1
1.7	547.4	109.7	94.1
2.0	3412.3	157.3	133.9

TABLE III. Number of gamma rays reaching Earth's surface from different heights above.

	H = 0 m	H = 50 m	H = 200 m	H = 500 m	H = 1000 m
N_γ	1106968	581764	466073	313161	185241

detectors increases from 50 to 200 m, the number of additional gamma rays decreases two times, and for 1000 m the number decreases three times.

Thus, Monte Carlo simulations demonstrate that even very small intracloud electric fields can lead to sizable enhancements in the gamma photon flux in the energy range of 0.3–3 MeV. We assume that the electric fields in the atmosphere do not decline abruptly after cessation of the severe storm and for many tens of minutes can supply the cosmic ray electrons with additional energy that leads to the enhanced probability of radiating bremsstrahlung gamma rays.

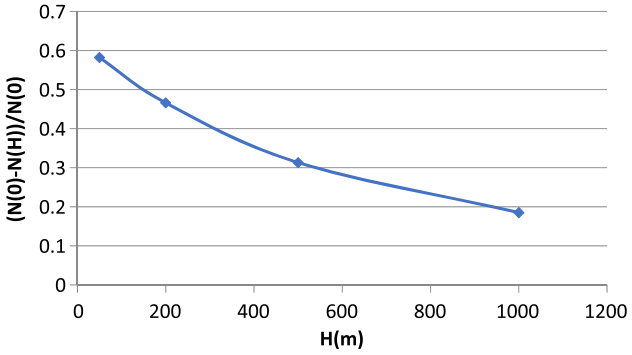

FIG. 6. The percentage of gamma rays reaching Earth's surface after escaping from an electric field at different heights (related to the case when the electric field is prolonged to Earth's surface). Ez = 0.8 kV/cm with an elongation of 1 km.

V. WINTER ENHANCEMENTS OF GAMMA RAY FLUX (WINTER TGES)

The winter is very severe on Aragats; the temperature on Aragats usually reaches −20 C° and stays deep in the negative domain until May. There is a strong positive correlation between temperature and radon emanation: at negative temperatures, radon concentration is strongly decreased [32]. The thickness of snow covering Aragats usually reaches and exceeds 1.5 m, which also may affect the ^{222}Rn concentration [33]. Thus, the radon emanation in the atmosphere is suppressed in winter. On the other hand, during snow storms with the presence of strong winds, radon can easily diffuse and reach particle detectors. Electric fields in winter are very weak; there are no lightning flashes, large disturbances of near-surface electric fields, or bursts of high-energy particles (gamma rays and electrons with energies up to 50 MeV). Thus, we do not observe any large enhancements during the winter. However, after precise scanning of the count rate monitoring results, we outline four events with particle flux enhancements in the NaI network. The detector network used to measure the particle energy spectra consists of six NaI crystal scintillators, each with a sensitive area of ∼0.0330 m^2 (∼5 times that of the ORTEC NaI). The energy resolution of spectrometers is 30%–40% at 662 KeV; thus we cannot resolve ^{222}Rn progeny spectral lines with these crystals. The big advantage of using large NaI crystals is the possibility to measure high-energy particles. A large count rate allows us to reliably measure a rather weak flux of high-energy electrons and gamma rays in the energy range above 10 MeV. In Fig. 7 we present 1-min time series of four winter TGEs observed by the NaI (Tl) network. In December the ORTEC spectrometer was located under the roof of the SKL experimental hall near the NaI network [Figs. 7(c) and 7(d)]; i.e., the ^{214}Bi isotope daily variations were minimal. In January the ORTEC spectrometer was moved outdoors [Figs. 7(a) and 7(b)] near the spectrometer used in [15]. For the outdoor location, the variation of the ^{214}Bi isotope concentration is significantly larger; see Fig. 3 (diamonds). The NaI network, as well as the ORTEC spectrometer, operates in two modes: measuring energy release histograms and, also, 1-min time series of count rates. Particle flux enhancement is apparently seen in all four events shown in Fig. 7.

In Fig. 8 we demonstrate the procedure of obtaining pure signal and demonstrate energy spectra for all four events.

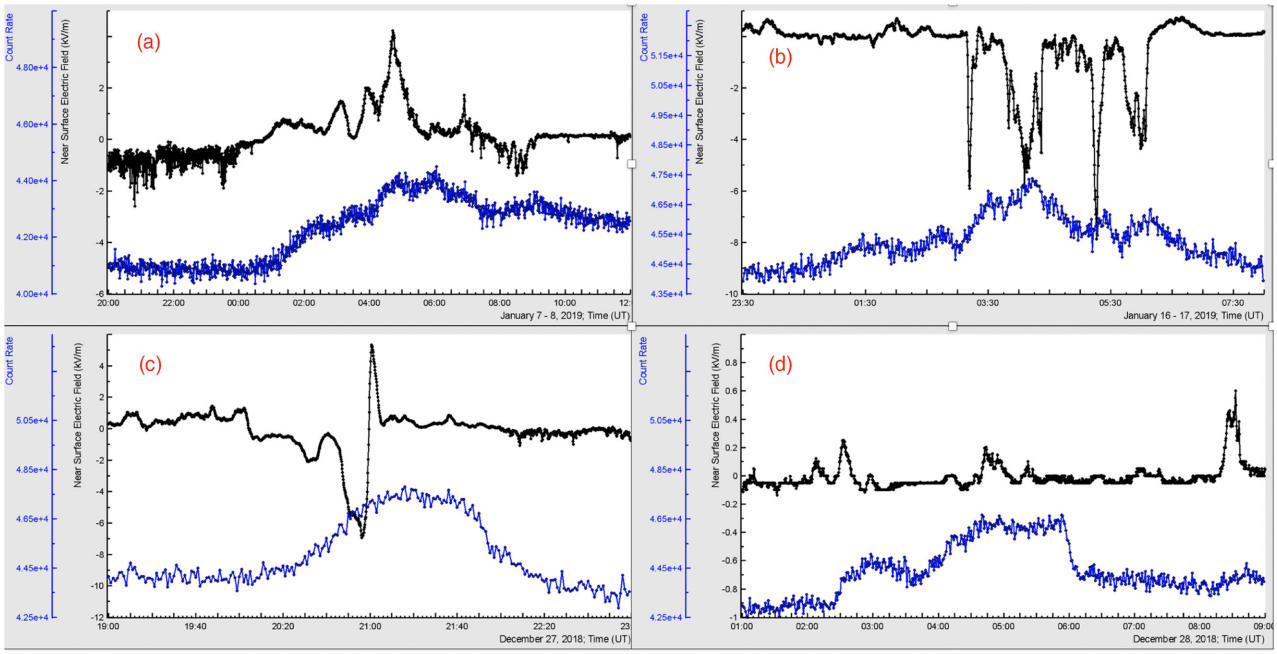

FIG. 7. Four observed events of particle flux enhancement in winter 2018/2019. Disturbances of the near-surface electric field (black curves). 1-min time series of count rates of particle flux measured by the first NaI crystal located under the roof of the SKL experimental hall on Aragats (blue curves).

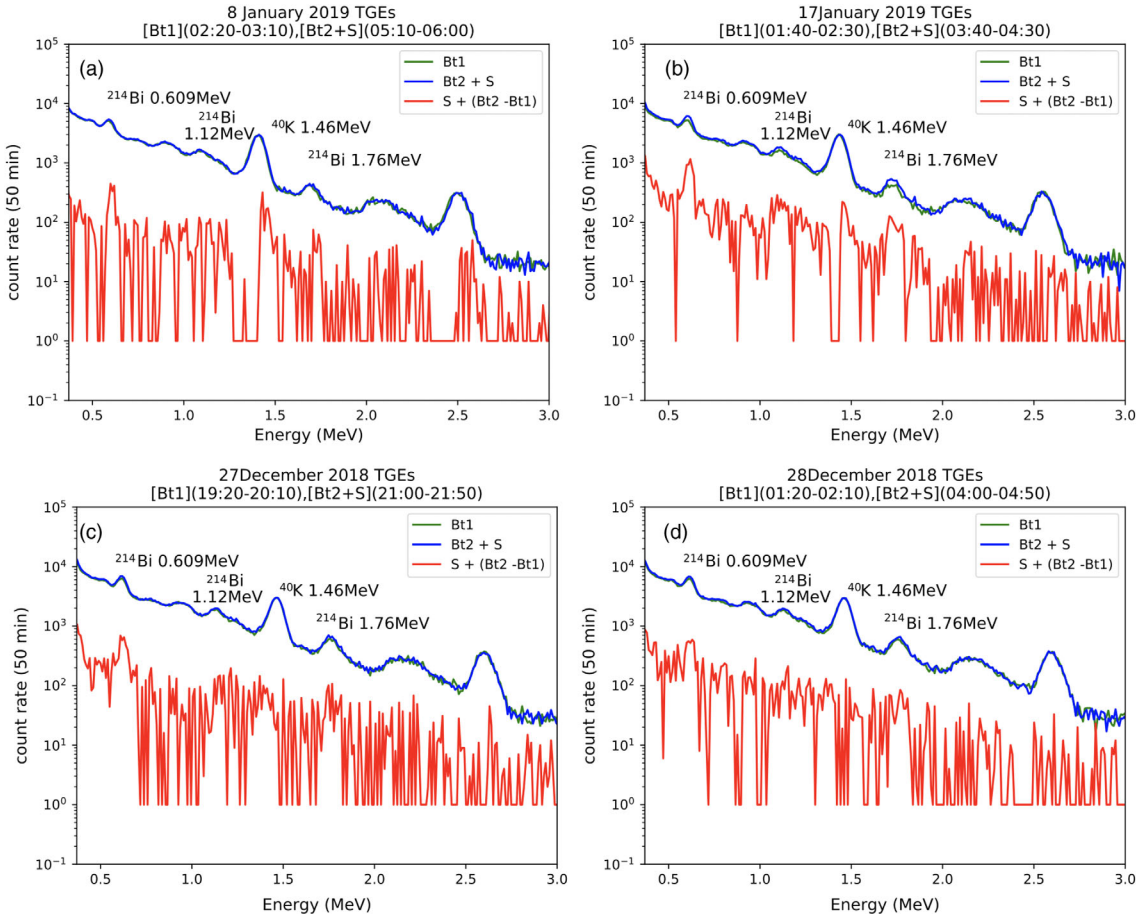

FIG. 8. Differential energy spectra of the winter TGEs measured (a), (b) in open air and (c), (d) in the SKL experimental hall.

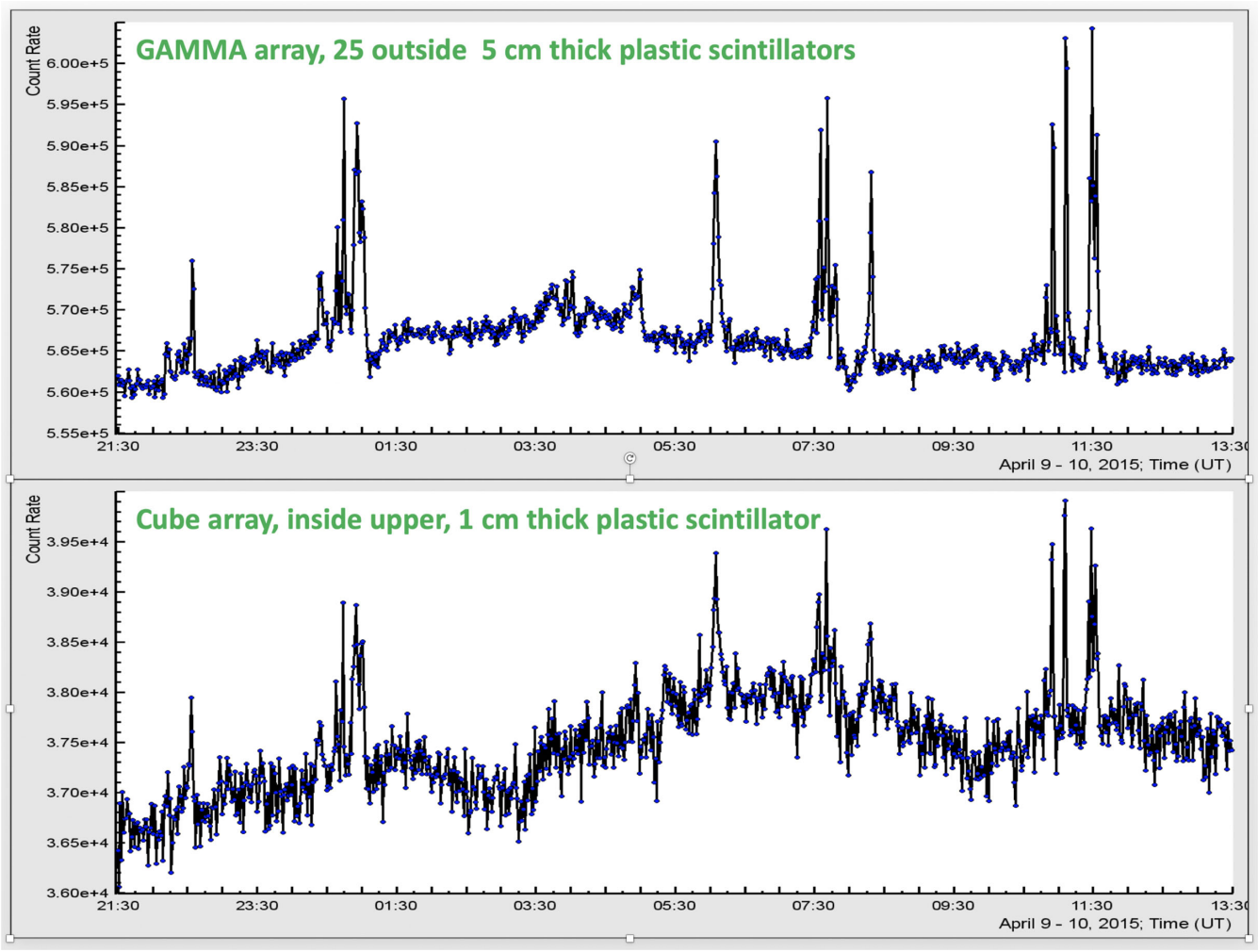

FIG. 9. The TGE measured by (upper) the 1-cm-thick and 1-m^2-area plastic scintillator of the indoor CUBE detector and by (lower) the 5-cm-thick and 25-m^2-area plastic scintillators of the GAMMA experiment.

Subtracting the background sample, we obtain an estimate of the pure signal used for the recovery of differential energy spectra with superimposed spectral lines originating from natural isotope gamma decay. The times of background (BT1) sampling and signal + background sampling (BT2 + S) were 50 minutes. The resulting signals obtained by subtracting background from the signal + background are shown in the lower part of frames (a)–(d) of Fig. 8. Obtained in such a way, the peak corresponding to the 0.609 KeV spectral line is seen in all four events. For the outdoor location of the spectrometer (January events) the 0.609 KeV peak is better pronounced and the peaks corresponding to the 1.12 and 1.76 MeV also can be outlined.

The continuum spectrum from cosmic rays is obscured by Compton scattered gamma rays escaping from the NaI crystal, forming another continuum spectrum to the left of the peaks corresponding to the spectral lines. There are no peaks corresponding to the stable ^{40}K line in December events [inside spectrometer location, Figs. 8(c) and 8(d)]; for the outside location of the spectrometer [Figs. 8(a) and 8(b)], a negative/positive profile of the ^{40}K line is detected. We connect this difference with high diurnal fluctuations of the isotope radiation in the open air possibly due to the outside temperature induced gain shift. For energies above 1.76 MeV, no spectral peaks for all four winter flux enhancements are seen. Thus, the measurements performed with the ORTEC spectrometer demonstrate that radon progeny radiation significantly contributes to the winter TGE events. A more detailed analysis of the ^{222}Rn progenies' contribution, as well as the contribution of the Compton scattered gamma ray's spectral lines, will be made after experiments with a high-precision HPGe spectrometer at Aragats planned for May 2019. In the next section, we will show that particles that form TGEs have energies well above the energetic domain where isotope decays can contribute to TGE count rate; thus the origin of TGEs is connected with electron acceleration in the

intracloud electric fields and not with gamma radiation from ^{222}Rn progenies.

VI. LONG-LASTING TGES MEASURED BY THE PLASTIC SCINTILLATORS

The particle flux monitoring on Aragats was performed by more than 200 detectors. Thus, we have the possibility to use several independently operated detectors to cross-check the flux enhancements. The first long-lasting TGEs observed on Aragats with a 3-cm-thick and 1-m^2-area plastic scintillator were reported in [34] in 2015; see Figs. 7, 9, and 10. We estimate the energies of the gamma rays responsible for the long-lasting enhancement with the notion of the "effective energy threshold" for gamma ray measurements introduced in [21]. According to this method, the energy threshold of a 3-cm-thick plastic scintillator is ∼3 MeV (see Fig. 10 of [21]). The contamination of TGE by radon progeny decay gamma rays as we demonstrate in the previous section is essential for energies below 3 MeV. Thus, the TGE observed by the 3-cm-thick plastics can originate from intracloud electric fields only (the MOS process). To confirm this observation, we present in Fig. 9 the same TGE measured by other scintillators: the 1-cm-thick scintillator of the CUBE array (effective energy threshold ∼1 MeV) and 25 scintillators of the GAMMA surface array, each 5 cm thick with an area of 1 m^2 (effective energy threshold ∼5 MeV). The TGEs presented in Fig. 9 well coincide with the TGEs published in 2016 and the enhancement of the count rate is proportional to the effective energy threshold.

In Figs. 10 and 11 we present other TGEs measured by plastic scintillators along with disturbances of the near-surface electric field obtained by the EFM-100 electric mills of the BOLTEK company. In both upper panels,

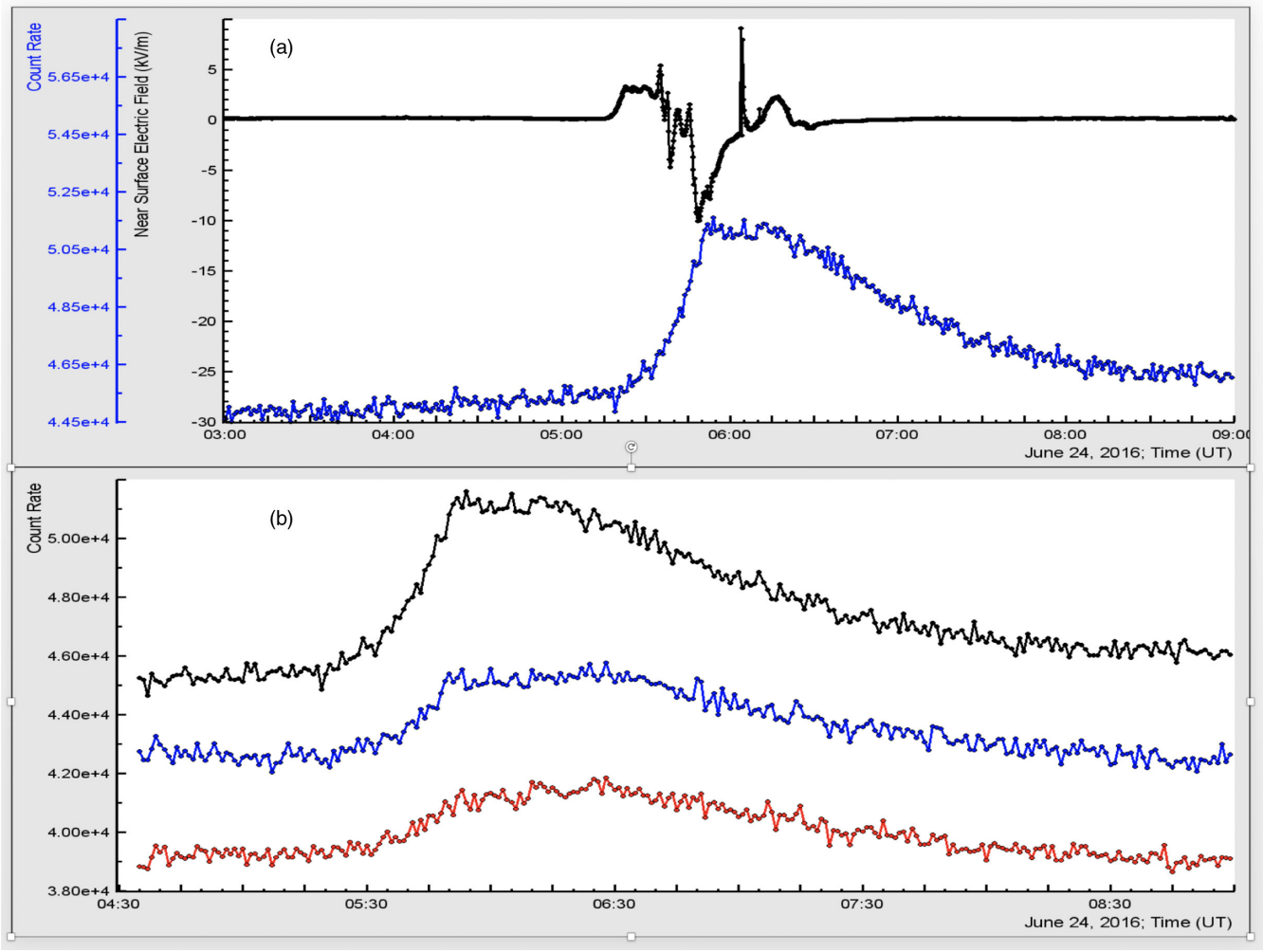

FIG. 10. (a) The disturbances of the electric field and count rate measured by the large crystal of the NaI network. (b) Comparison of the count rate time series measured by the same crystal and two vertically stacked plastic scintillators of the STAND1 detector, with a thickness of 1 cm and an area of 1 m^2, located outdoors near the MAKET experimental hall.

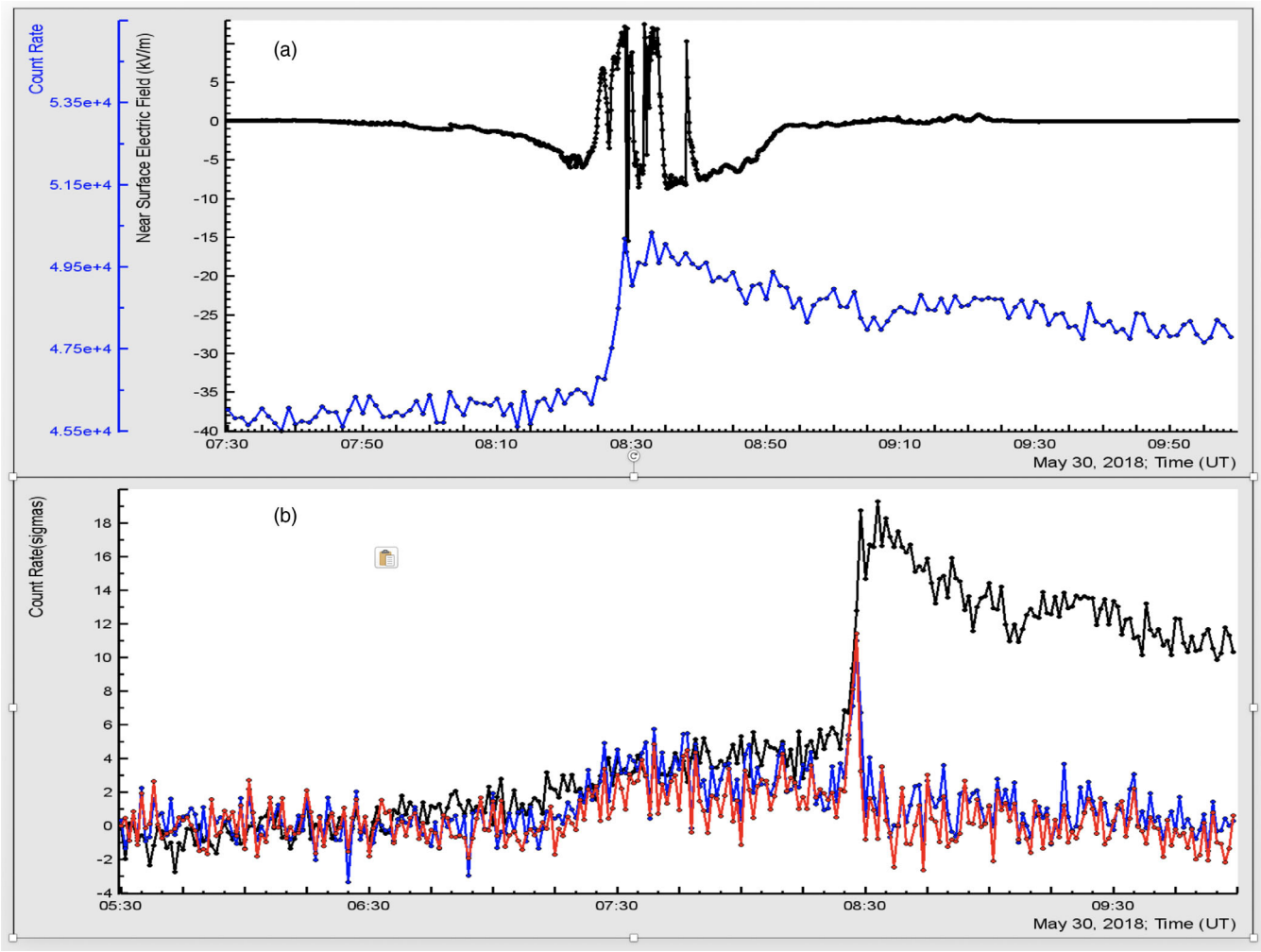

FIG. 11. (a) The disturbances of the electric field and count rate measured by the large crystal of NaI network. (b) One-minute count rates of the same NaI crystal and count rates of the upper and middle of the vertically stacked scintillators of the STAND3 detector located indoors in the SKL experimental hall. The count rate in the panel (b) is shown in the number of standard deviations from the mean count rate measured before TGE to fit in one picture time series of two detectors that are significantly different in the count rates.

Figs. 10(a) and 11(a), we see that both TGEs are directly related to the large disturbances of the electric field. In Figs. 10(b) and 11(b) we demonstrate the TGEs as measured by the NaI crustal and by plastic scintillators. The shapes of all curves measured by detectors with different energy thresholds are very similar; thus, we can conclude that the physical mechanism responsible for the TGE initiation is one and the same. As the energy threshold of plastic scintillators [middle scintillator of STAND1, the lower curve in Fig. 10(b), and middle scintillator of STAND3, the lower curve in Fig. 11(b)] is above 3 MeV, we can confirm the "electric" origin of the shown TGEs. In Figs. 10 and 11 we can also see that enhancement of the count rate starts simultaneously with disturbances of the electric field. For the TGE measured on May 30 (Fig. 11) an abrupt rise in NaI crystal count rate coincides with the sharp decrease of electric field and occurrence of high-energy particles in the TGE.

In Fig. 12 we demonstrate the recovered energy spectra of particle flux enhancement on January 17, 2019, and during the TGE that occurred on March 4, 2016. The data collecting time was 50 minutes for each of the two events. In the previous section, we explain the January 17 event by the ^{222}Rn progeny gamma radiation and in Fig. 12(a) we can see that the energy spectrum is continued until 3 MeV only. On the other hand, the energy spectrum of the TGE measured on March 2, 2016 [Fig. 12(b)], continued up to 10 MeV, where the radon progenies surely cannot contribute. Thus, we relate the gamma rays registered on March 2, 2016, with energies above 3 MeV to RREA and MOS processes in the intracloud electric fields.

Thus, the electric nature of TGEs can be derived from the observations with plastic scintillators of various thicknesses and different energy thresholds, as well as by observing energy spectra prolonged far beyond 3 MeV.

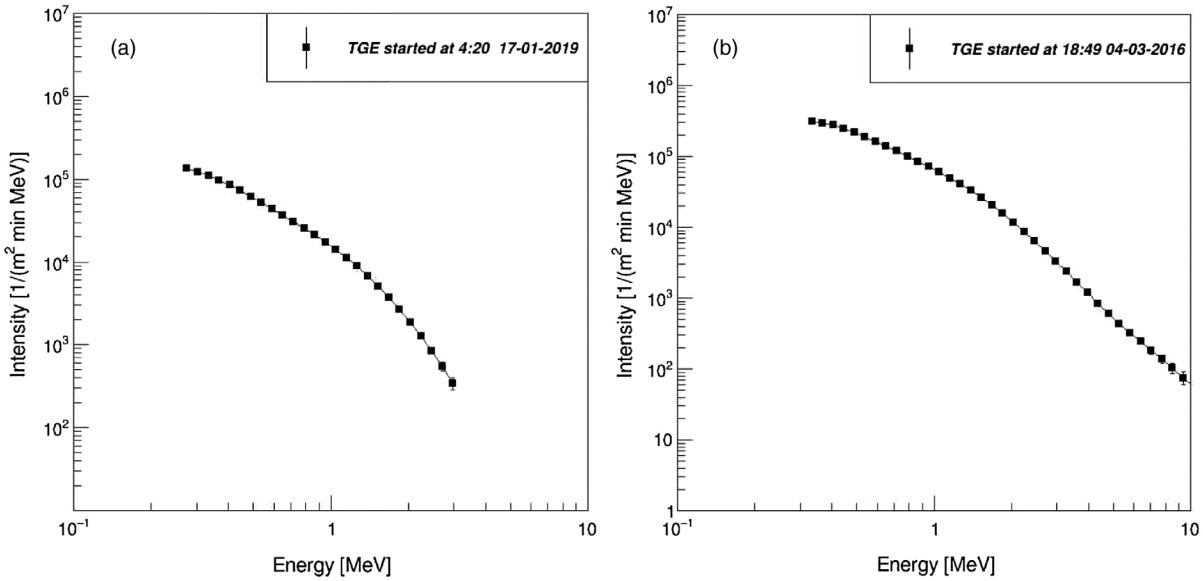

FIG. 12. Differential energy spectra of (a) the winter enhancement that occurred on January 17, 2019, and (b) the TGE that occurred on March 4, 2016, during a strong thunderstorm. The energy release histograms were collected by four NaI crystals (see details in [35], Fig. 4) over 50 min.

VII. CONCLUSIONS

In December and January of the 2018–2019 winter, we performed monitoring of the particle count rate with a precise NaI(Tl) ORTEC spectrometer (FWHM ∼7.7% at 0.6 MeV) and with a NaI crystal network. All spectrometers recorded prolonged periods of gamma ray enhancements. Two locations of the ORTEC spectrometer were included in data analysis: under the roof of the SKL experimental hall, where the Aragats NaI network is located, and in open air near the spectrometer used in [15].

The analysis of the four winter TGEs allowed us to confirm the significant contribution of the gamma radiation from radon progenies to the count rate enhancement in the energy range below 3 MeV in the winter.

This result should be confirmed by observation of much more intense spring TGEs incorporating also a precise HPGe spectrometer. Comparing spectra measured by NaI and Ge spectrometers will allow us to estimate the portion of Compton scattered gamma rays forming a continuous spectrum on the left of the isotope gamma radiation lines.

By measurements with plastic scintillators and by performing Monte Carlo simulations we confirm the electric nature of the long-lasting TGEs. TGEs observed by the plastic scintillators demonstrate that the extended enhancements of the particle flux are related to energies above 3 MeV, where radon progenies cannot contribute to the TGE counts.

CORSIKA code was used to investigate the small fields effect on particle detector count rates. We show that even for not very large values of the atmospheric electric field strengths, modification of the cosmic ray electron energy spectra (the MOS process [8]) leads to bremsstrahlung radiation sustaining additional gamma ray flux.

Each TGE observed on Aragats is accompanied by disturbances of the near-surface electric field and, in turn, each disturbance of the electric field has its roots in the enhanced concentration of hydrometeors above the station. Modeling with the WRF code proves the existence of charged layers above the station simultaneously with TGE detection [36]. Thus, the electrical origin of TGE is supported by theory, modeling, and observations of particle fluxes, electric fields, atmospheric discharges, and hydrometeor concentrations (microphysics).

ACKNOWLEDGMENTS

The data for this paper are available via the multivariate visualization software ADEI in the web page of the Cosmic Ray Division (CRD) of the Yerevan Physics Institute [37]. We thank the staff of the Aragats Space Environmental Center for installation and maintenance of the Na(Tl) spectrometer and the staff of Isotope Research Department for performing measurements with the HPGe spectrometer. We are thankful to Pokhsraryan David for the modernization of spectrometer software. The authors thank Ekaterina Svechnikova for modeling with wrf code the density of hydrometeors above Aragats. We appreciate the support of a Russian Science Foundation Grant (Project No. 17-12-01439).

[1] J. R. Dwyer, D. M. Smith, and S. A. Cummer, High-energy atmospheric physics: Terrestrial gamma-ray flashes and related phenomena, Space Sci. Rev. **173**, 133 (2012).

[2] A. Chilingarian, A. Daryan, K. Arakelyan, A. Hovhannisyan, B. Mailyan, L. Melkumyan, G. Hovsepyan, S. Chilingaryan, A. Reymers, and L. Vanyan, Ground-based observations of thunderstorm-correlated fluxes of high-energy electrons, gamma rays, and neutrons, Phys. Rev. D **82**, 043009 (2010).

[3] A. Chilingarian, G. Hovsepyan, and A. Hovhannisyan, Particle bursts from thunderclouds: Natural particle accelerators above our heads, Phys. Rev. D **83**, 062001 (2011).

[4] G. J. Fishman, P. N. Bhat, R. Mallozzi *et al.*, Discovery of intense gamma-ray flashes of atmospheric origin, Science **264**, 1313 (1994).

[5] M. McCarthy and G. Parks, Further observations of X-rays inside thunderstorms, Geophys. Res. Lett. **12**, 393 (1985).

[6] N. A. Kelley, D. M. Smith, J. R. Dwyer, M. Splitt, S. Lazarus, F. Martinez-McKinney, B. Hazelton, B. Grefenstette, A. Lowell, and H. K. Rassoul, Relativistic electron avalanches as a thunderstorm discharge competing with lightning, Nat. Commun. **6**, 7845 (2015).

[7] J. R. Dwyer, A fundamental limit on electric fields in air, Geophys. Res. Lett. **30**, 2055 (2003).

[8] A. Chilingarian, B. Mailyan, and L. Vanyan, Recovering of the energy spectra of electrons and gamma rays coming from the thunderclouds, Atmos. Res. **1**, 114 (2012).

[9] D. Sarria, C. Rutjes, G. Diniz *et al.*, Evaluation of Monte Carlo tools for high-energy atmospheric physics II: Relativistic runaway electron avalanches, Geosci. Model Dev. **11**, 4515 (2018).

[10] A. V. Gurevich, G. M. Milikh, and R. A. Roussel-Dupre, Runaway electron mechanism of air breakdown and preconditioning during a thunderstorm, Phys. Lett. **165A**, 463 (1992).

[11] J. R. Dwyer, Relativistic breakdown in planetary atmospheres, Phys. Plasmas **14**, 042901 (2007).

[12] L. P. Babich, E. N. Donskoy, I. M. Kutsyk, A. Y. Kudryavtsev, R. A. Roussel-Dupre, B. N. Shamraev, and E. M. D. Symbalisty, Comparison of relativistic runaway electron avalanche rates obtained from Monte Carlo simulations and kinetic equation solution, IEEE Trans. Plasma Sci. **29**, 430 (2001).

[13] L. I. Dorman and I. V. Dorman, Possible influence of cosmic rays on climate through thunderstorm clouds, Adv. Space Res. **35**, 476 (2005).

[14] A. Chilingarian, Thunderstorm ground enhancements—model and relation to lightning flashes, J. Atmos. Sol. Terr. Phys. **107**, 68 (2014).

[15] V. V. Bogomolov, A. F. Iyudin, I. A. Maximov *et al.*, Detection of Rn-222 daughter radiation during long lasting thunderstorm ground enhancements on mountain Aragats, Phys. Rev. D (to be published).

[16] A. Chilingarian, Long lasting low energy thunderstorm ground enhancements and possible Rn-222 daughter isotopes contamination, Phys. Rev. D **98**, 022007 (2018).

[17] A. Chilingarian, G. Hovsepyan, S. Soghomonyan *et al.*, Structures of the intracloud electric field supporting origin of long-lasting thunderstorm ground enhancements, Phys. Rev. **98**, 082001 (2018).

[18] T. Enoto, Y. Wada, Y. Furuta *et al.*, Photonuclear reactions triggered by lightning discharge, Nature (London) **551**, 481 (2017).

[19] A. Chilingarian, G. Hovsepyan, and B. Mailyan, *In situ* measurements of the runaway breakdown (RB) on Aragats mountain, Nucl. Instrum. Methods Phys. Res., Sect. A **874**, 19 (2017).

[20] A. Chilingarian, Energetic radiation from thunderclouds: Extended particle fluxes directed to Earth's surface, https://doi.org/10.1007/s12210-018-0755-y.

[21] A. Chilingarian, S. Chilingaryan, and G. Hovsepyan, Calibration of particle detectors for secondary cosmic rays using gamma-ray beams from thunderclouds, Astropart. Phys. **69**, 37 (2015).

[22] T. Gesell, Background atmospheric ^{222}Rn, concentrations outdoors and indoors: A review, Health Phys. **45**, 289 (1983).

[23] F. Corvalno, Origins and concentrations of ^{222}Rn, ^{210}Pb, ^{210}Bi and ^{210}Po in the surface air at Lisbon, Portugal, at the Atlantic edge of the European continental landmass, Atmos. Environ. **29**, 1809 (1995).

[24] I. Sýkora, M. Ješkovský, R. Janík, K. Holý, M. Chudý, and P. P. Povinec, Low-level single, and coincidence gamma-ray spectrometry, J. Radioanal. Nucl. Chem. **276**, 779 (2008).

[25] H. E. Moore, S. E. Pet, and E. A. Martell, ^{222}Rn^{210}Bi, and ^{210}Po, ^{214}Bi profiles and aerosol residence times versus altitude, J. Geophys. Res. **78**, 7065 (1973).

[26] I. Hossain, N. Sharip, and K. K. Viswanathan, Efficiency and resolution of HPGe and NaI(Tl) detectors using gamma-ray spectroscopy, Sci. Res. Essays **7**, 86 (2012).

[27] P. Blum, Physical Properties Handbook: A Guide to the Shipboard Measurement of Physical Properties of Deep-Sea Cores (College Station, Texas, USA, 1997), http://www-odp.tamu.edu.

[28] J. R. Letaw, G. H. Share, R. L. Kinzer, R. Silberberg, E. L. Chupp, D. J. Forrest, and E. Rieger, Satellite observation of atmospheric nuclear gamma radiation, J. Geophys. Res. **94**, 1211 (1989).

[29] A. Chilingarian, J. Knapp, and M. Zazyan, Atmospheric monitoring for high energy astroparticle detectors (AtmoHEAD-2018), EPJ Web Conf. 197, 2 (2019).

[30] T. C. Marshall, M. Stolzenburg, C. R. Maggio *et al.*, Observed electric fields associated with lightning initiation, Geophys. Res. Lett. **32**, L03813 (2005).

[31] T. C. Marshall, M. Stolzenburg, P. R. Krehbiel *et al.*, Electrical evolution during the decay stage of New Mexico thunderstorms, J. Geophys. Res. **114**, D02209 (2009).

[32] D. E. Tchorz-Trzeciakiewicz and A. T. Solecki, Seasonal variation of radon concentrations in atmospheric air in the Nowa Ruda area (Sudety Mountains) of southwest Poland, Geochemical Journal **45**, 455 (2011).

[33] R. Fujiyoshi, H. Morimoto, and S. Sawamura, Investigation of the soil radon variation during the winter months in Sapporo, Jpn. Chemosphere **47**, 369 (2002).

[34] A. Chilingarian, G. Hovsepyan, and L. Kozliner, Extensive air showers, lightning, and thunderstorm ground enhancements, Astropart. Phys. **82**, 21 (2016).

[35] A. Chilingarian, G. Hovsepyan, and E. Mantasakanyan, Mount Aragats as a stable electron accelerator for atmospheric high-energy physics research, Phys. Rev. D **93**, 052006 (2016).

[36] E. K. Svechnikova, N. V. Ilin, and E. A. Mareev, Recovery of electrical structure of the cloud with use of ground-based measurement results, *Proceeding of TEPA-2018 Conference, Nor-Amberd, Armenia, 2018* (Tigran Mets, Yerevan, 2019).

[37] Advanced Data Extraction Infrastructure, http://adei.crd.yerphi.am/adei.